Article

The Role of Ozone in the Reaction Mechanism of a Bare Zeolite-Plasma Hybrid System

Yoshiyuki Teramoto *, Hyun-Ha Kim, Nobuaki Negishi and Atsushi Ogata

National Institute of Advanced Industrial Science and Technology (AIST),
16-1 Onogawa, Tsukuba 305-8569, Japan; E-Mails: hyun-ha.kim@aist.go.jp (H.-H.K.);
n-negishi@aist.go.jp (N.N.); atsushi-ogata@aist.go.jp (A.O.)

* Author to whom correspondence should be addressed; E-Mail: yoshiyuki-teramoto@aist.go.jp;
Tel.: +81-29-861-8715; Fax: +81-29-861-8866.

Academic Editor: Jean-François Lamonier

Abstract: We investigated the reaction mechanism of a metal-unloaded zeolite-plasma hybrid system for decomposition of toluene at room temperature. Short-lived radicals and fast electrons did not contribute substantially to the reaction mechanism of toluene decomposition in the zeolite-plasma hybrid system. The main factor enhancing the reaction mechanism was gas-phase O_3 directly reacting with toluene adsorbed onto the zeolite (the Eley-Rideal mechanism). CO_2 selectivity was not improved by using H-Y zeolite due to its low ability to retain the active oxygen species formed by O_3. The gas-phase O_3 reacted with adsorbed toluene to form a ring cleavage intermediate that was slowly converted into formic acid. The decomposition rate of formic acid was much lower than that of toluene on the H-Y surface.

1. Introduction

Non-thermal plasma processes have attracted significant interest as promising technologies for decomposing volatile organic compounds (VOCs) [1]. Over the last decade, research has focused on improving the process efficiency of decomposition of VOCs using various plasma reactors such as pulsed corona [2–4], ferroelectric pellet packed-bed discharge [5], silent (dielectric barrier) discharge [6], and surface discharge [7,8] reactors. The feasibility of plasma processes is limited by

energy efficiency and formation of toxic by-products. To improve energy efficiency and CO_2 selectivity, catalyzed hybrid plasma reactors have been designed [9–11]. For example, it has been reported that the combination of dielectric barrier discharge and a metal loaded catalyst enhances trichloroethylene decomposition and CO_2 selectivity [12,13]. Loading of active metals not only enhances CO_2 selectivity for various VOCs [9,14,15], but also improves plasma coverage on the surface [16]. We have also proposed a non-thermal plasma reactor combined with a catalyst [8,17] and cyclic plasma operation [18]. Plasma induced surface oxygen species on metal nanoparticles play a significant role in improvement of the process [19,20]. In particular, O_3 enhances formation of active oxygen species on the catalyst surface. Manganese oxides (MnO_x) are well known as promising catalysts for decomposition of VOCs by O_3 at low temperatures through the Langmuir-Hinshelwood (L-H) mechanism, as follows [21]:

$$O_3 + * \rightarrow O_2 + *O_{ads} \tag{1}$$

$$*O_{ads} + VOC_{ads} \rightarrow CO_x + H_2O + * \tag{2}$$
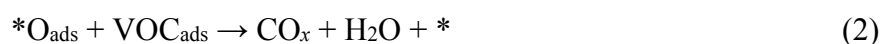
where $*$ is an active sites on the catalyst and $*O_{ads}$ is the active oxygen species on the catalyst. Previous studies have reported that metal nanoparticles on zeolite strongly retain the active oxygen species formed by plasma compared with bare zeolite. We previously investigated active oxygen species formed by plasma on a silver nanoparticle-loaded zeolite [22]. The amount of active oxygen fixed onto the catalyst surface by O_2 plasma was approximately proportional to the square of the amount of supported silver. Thus, most of the active oxygen was present on the silver surface. Interestingly, the ozone demand factor ($DF_{O3} = \Delta[O_3]/\Delta[toluene]$), *i.e.*, the amount of ozone required for oxidation of toluene of bare zeolite (ZSM-5), was half that of silver-loaded zeolite [23]. Smaller DF_{O3} values correlate with better performance during ozone-assisted catalysis of VOCs. These findings suggest that the supported metal does not necessarily improve the efficiency of the plasma hybrid system and that performance improvements in that system cannot be explained solely by surface reactions of active oxygen species formed by O_3 (the L-H mechanism).

In this study, we focused on reaction mechanisms of a metal-unloaded zeolite in a plasma hybrid system for toluene decomposition. The role of metal nanoparticles has been studied by several research groups and has been found to be important in VOC removal, affecting decomposition efficiency, the carbon balance, and CO_2 selectivity. However, the role of supports (e.g., without active metals) has not been well studied in terms of interaction with plasma. The role of zeolite in the toluene decomposition process was investigated by changing the position of the zeolite in the plasma reactor. The reaction mechanisms of toluene decomposition in the gas phase and on the zeolite surface were studied using gaseous and surface FT-IR analyses.

2. Results and Discussion

2.1. Role of Zeolites in the Plasma Hybrid System

Energy efficiency in the decomposition of VOCs was enhanced by using a zeolite-hybrid plasma reactor [18]. Improvements in efficiency differed widely depending on the type of zeolite and its position in the reactor. Table 1 summarizes the performance of the zeolites in toluene oxidation, and their basic properties. Decomposition efficiency in the downstream position was 3.7 times higher than that in a

conventional reactor, while that in the upstream position was 1.2–1.5 times higher. Additionally, decomposition efficiency in the downstream position was significantly affected by the type of zeolite, compared with upstream. The dependence of the decomposition efficiency on the position of the zeolite suggests that improvements in performance cannot be explained solely by activation of the zeolite surface by plasma.

Table 1. Decomposition efficiency in hybrid plasma reactors and the properties of zeolites.

Zeolite	C₇H₈ decomposition (%)		Product selectivity (%)						Carbon balance (%)		Surface area (m²/g)	SiO₂/Al₂O₃	Channel (Å)
			CO		CO₂		HCOOH						
None	15		35		48		17		97		-	-	-
Na-Y	Upstream 21	Downstream 52	36	33	56	63	8	4	95	92	750	3.1	7.4
H-Y(1)	18	55	41	45	52	47	7	8	97	99	650	1.9	7.4
H-Y(2)	20	50	47	42	46	51	7	7	98	96	520	5.6	7.4
MOR	23	35	46	42	45	52	9	6	97	96	460	15.2	6.7 × 7.0
FER	19	20	38	33	49	65	13	2	96	99	270	17.9	4.3 × 5.5

Figure 1 shows the relationship between the amount of toluene adsorbed and decomposition efficiency (normalized to that of a reactor without zeolites). In general, the surface area greatly affects the adsorption capacity and decomposition of VOCs. In a previously reported ozone-assisted catalyst system, the rate of benzene oxidation linearly increased with the specific surface area of the MnO_x-loading catalyst, regardless of the type of catalyst support [24]. In the present study, the amount of toluene (~6 Å) adsorbed by ferrierite (FER) was small and limited to the surface due to the micropore size (4.3×5.5 Å²) of FER.
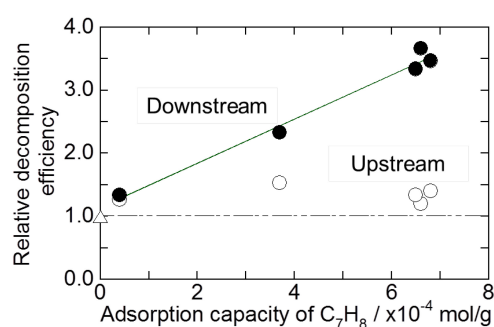

Figure 1. Relationship between the decomposition efficiency and adsorption capacity for toluene.

The decomposition efficiency of the downstream configuration was linearly proportional to the adsorption capacity (Figure 1). On the other hand, that of the upstream configuration was near constant. If the toluene adsorbed in the internal areas of the zeolite was decomposed by short-lived radicals and fast electrons, the decomposition efficiency would not depend on the zeolite position. We conclude that reactions between toluene adsorbed onto the zeolite and short-lived radicals or fast electrons did not contribute to improvements in decomposition efficiency. One possible explanation is the limited area of plasma for bare zeolite compared to metal-loaded zeolites; plasma mainly formed at the points of contact with the zeolite pellets [16]. This limited plasma area reduced effective interactions at the surface of the zeolite. These results confirm the important contribution of metal nanoparticles to both plasma properties and catalytic performance.

In addition, the diffusion lengths of short-lived radicals (O and OH) and fast electrons are <100 μm at atmospheric pressure. Thus, short-lived radicals and fast electrons had limited effect in this system.
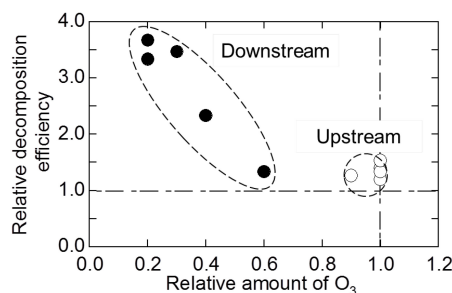

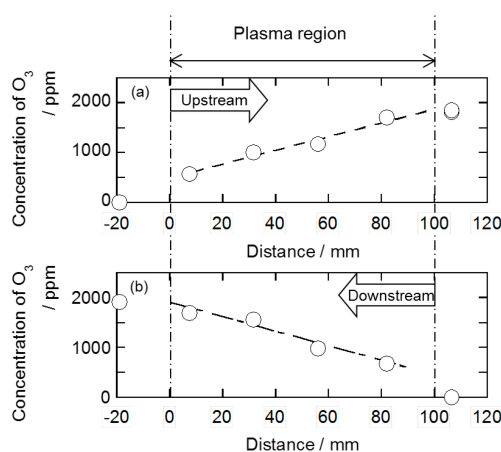**Figure 2.** Relationship between the relative decomposition efficiency and relative amount of ozone.

Figure 3. Ozone distribution in a conventional plasma reactor: (**a**) upstream configuration and (**b**) downstream configuration.

Ozone has a long diffusion length (>10 mm) due to its long lifetime, and can reach the inner area of micropores. Figure 2 shows the decomposition efficiency as a function of the outlet O_3 concentration, normalized to that of a reactor without zeolites. In the downstream position, the O_3 concentration was affected by the type of zeolite and decreased with increasing decomposition efficiency. Therefore, O_3 was consumed approximately linearly with toluene oxidation. In the upstream position, there were no significant differences in O_3 concentration or decomposition efficiency among the zeolite types. This can be explained by the O_3 concentration at the entrance of the plasma reactor. The distribution of O_3 concentrations in the reactor tube were measured using a dedicated reactor (shown in section 3.2.). Figure 3a,b shows the distribution of O_3 in an unfilled reactor under dry air flow (without toluene or H_2O) in the upstream and downstream configurations, respectively. The O_3 concentration increased linearly with distance from the entrance of the reactor in both directions. When 1.0 g of H-Y was placed in the upstream or downstream position, the O_3 concentration remained constant in the zeolite-filled region (Figure 4a,b)). These results were also observed for other zeolite types. Thus, formation of O_3 was strongly suppressed in the zeolites-filled region. Based on these results, the low decomposition efficiency of the upstream configuration was likely due to a low O_3 concentration, while the high efficiency of the downstream configuration was due to a high O_3 concentration. Therefore, adsorbed

toluene in the internal area of the zeolite was manly decomposed by O_3. In addition to reactions (1) and (2), the following reaction represents this mechanism:
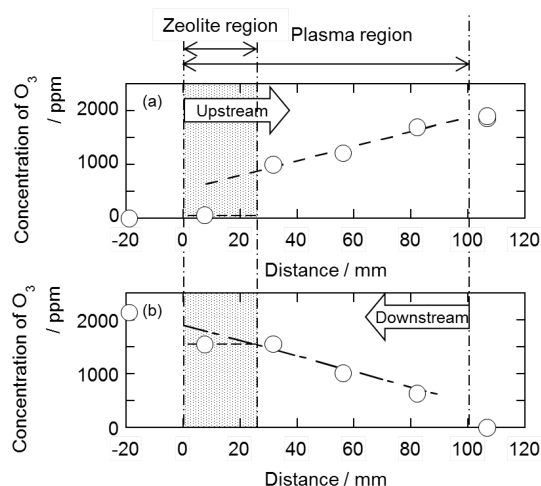
$$*VOC_{ads} + O_3 \rightarrow CO_x + H_2O + * \tag{3}$$

Figure 4. Relationship between the decomposition efficiency and the adsorption of ozone: (**a**) upstream configuration and (**b**) downstream configuration.

In reactions (1) and (2), O_3 initially decomposes at the zeolite surface. Figure 5 shows the outlet concentration of O_3 in the downstream reactor filled with 1.0–3.0 g of H-Y. No decomposition of O_3 was observed for any case. Thus, H-Y has little ability to decompose O_3 and form active oxygen species on its surface. Therefore, the main process involved in toluene decomposition is likely direct reaction of gas phase O_3 with toluene adsorbed onto H-Y, *i.e.*, the Eley-Rideal (E-R) mechanism. This process is different from that for other types of zeolites and metal-loaded zeolites, *i.e.*, the L-H mechanism. For example, active oxygen species formed by O_3 on the MCM-41 and MS-13X surfaces significantly contributed to VOC decomposition [25,26]. These active oxygen species on the catalyst surface are consumed in reactions with VOCs, O_3, O, *etc.* [27–29]. In other words, some of the active oxygen species (=O_3) form unwanted byproducts in the L-H process, unlike in E-R. Therefore, in the E-R process, the H-Y zeolite has the potential for achieving low DF_{O3} in VOC decomposition.
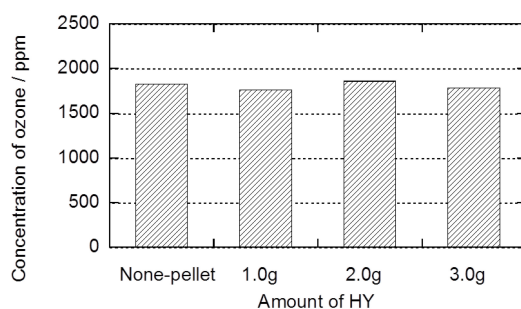

Figure 5. Concentration of ozone in the downstream reactor with amount of H-Y(1).

CO_2 selectivity was similar between the H-Y filled and unfilled reactors (Table 1). On the other hand, production of formic acid was lower for the H-Y filled reactors. Considering the role of O_3 in this system (reaction (3)), it may be difficult for gaseous O_3 to oxidize the adsorbed CO to CO_2, unlike for toluene

and formic acid. Generally, in a plasma-catalyst hybrid system, bare zeolite contributes little to oxidization of CO. Metal-loaded zeolites significantly improves CO_2 selectivity due to surface reaction with the active oxygen species formed by O_3, most of which are present on the silver surface of the catalyst [22]. Thus, active oxygen species on the metal surface contribute greatly to improvements in CO_2 selectivity. The H-Y zeolite cannot easily retain active oxygen species on its surface through reactions with O_3, leading to low CO_2 selectivity.

Higher concentrations of VOCs result in higher energy efficiencies for removal [30]. Kuroki *et al.* [31] reported that adsorbed toluene desorbed easily by DC pulsed plasma discharge, resulting in an increase in the concentration of VOCs. Although this experimental result using standard adsorbents cannot be directly compared with zeolites, if such an effect occurred in our system, the efficiency in the upstream reactor should be nearly the same as that in the downstream one. However, efficiency in the downstream configuration was much higher than that in the upstream reactor. This suggested that enhancement due to desorption of toluene from the zeolite was negligible.

The hydrophilicity of zeolite depends on the SiO_2/Al_2O_3 ratio and affects the performance of thermal catalytic processes. Generally, hydrophilicity decreases with increasing SiO_2/Al_2O_3 ratio. However, the difference in hydrophilicity between H-Y(1) and H-Y(2) did not affect decomposition efficiency in our system (Table 1), unlike for thermal catalytic processes.

2.2. Decomposition of Toluene Adsorbed onto the Zeolites by O_3

Figure 6a,b shows spectra for toluene adsorbed onto H-Y and FER, respectively, measured 10 min after introducing 200 ppm of toluene in N_2. Figure 6c also shows the spectrum for toluene in the gas phase as a reference. IR peaks assigned to the aromatic ring were observed between 2000 and 1750 cm^{-1} in both Figure 6a,b. These peak positions were shifted compared with those in the gas phase. Table 2 summarizes the IR peaks for toluene in both the gas and liquid phases. The adsorption peaks near 3000 cm^{-1} were assigned to the CH_3 group of toluene and those at 2000–1700 cm^{-1} were assigned to the C–H bonds in the aromatic ring. The shift in peaks for toluene adsorbed onto the zeolite is due to the perturbation of the π-electric system by adsorption onto the H-Y zeolite. These peaks were assigned to toluene physically adsorbed onto the solid surface, because they completely disappeared upon heating the sample to 200 °C. The peak signal for toluene on FER was much smaller than that on H-Y, because the adsorption capacity of FER for toluene is limited due to its small micropore size.
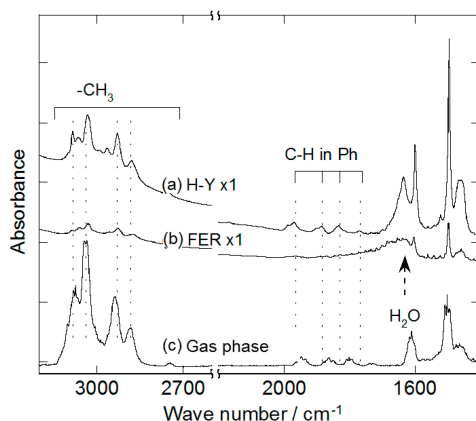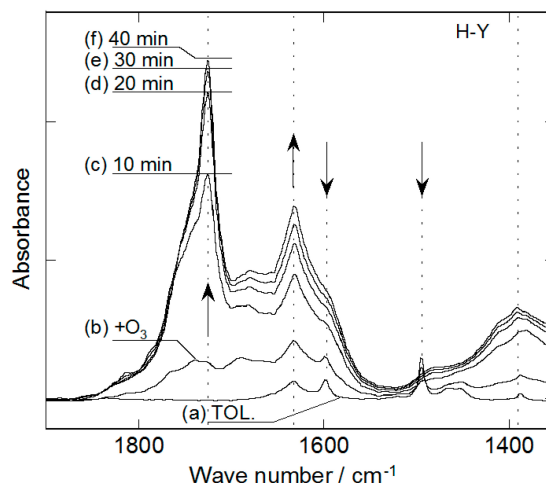

Figure 6. Infrared spectra for toluene (**a**) on H-Y(1) zeolite, (**b**) on FER, and (**c**) in the gas phase.

Table 2. Wave number of IR peaks for toluene in gas phase, in the liquid film, and on H-Y.

Bond	Gas phase	Liquid film	on H-Y
	3101	3087	3083
C–H in Ph	3076	3062	3065
	3037	3026	3031
	-	2948	2963
C–H in CH_3	2938	2920	2928
	2881	2873	2879
	1942	1942	1969
C–H in Ph	1856	1858	1884
	1801	1803	1832
	1732	-	1772
	1611	1605	1599
C–C in Ph	-	1524	-
	1500	1496	1495
	1463	1451	1457
	Infra-red DB	SDBS	this work

The reactivity of toluene adsorbed onto H-Y was then investigated. Initially, toluene was adsorbed onto the H-Y sample for 10 min (Figure 7a). N_2 gas was then supplied to remove the gas phase toluene from the reactor. A mixture of 400 ppm O_3 in O_2 was then introduced and the FT-IR spectrum was recorded (Figure 7b–f). The IR peaks for toluene disappeared immediately after O_3 introduction, in less than 1 min. In contrast, IR peaks at 1390, 1630 and 1725 cm^{-1} appeared and their intensities increased for 40 min after O_3 introduction. These peaks were assigned to formic acid (HCOOH). These results suggest that gas-phase O_3 reacted with adsorbed toluene to form ring cleavage intermediate that was slowly converted to formic acid. We anticipate that the performance of the zeolite-plasma hybrid system could be improved by increasing the operating temperature, because the decomposition rate of formic acid is significantly affected by temperature [18].

Figure 7. Infrared spectra for toluene decomposition on H-Y(1): (**a**) toluene adsorbed onto H-Y; after addition of O_3 for (**b**) 0, (**c**) 10, (**d**) 20, (**e**) 30, and (**f**) 40 min.

A distinctive peak for the active oxygen species formed by O_3 on MCM-41 and MS-13X was observed at around 1380 cm^{-1} [25,26]. In the present experiment, this peak was not observed. This result supports the observation that the H-Y zeolite does not retain active oxygen species on its surface through reaction with O_3.

Figure 8 shows IR spectra for formic acid adsorbed to H-Y for 10 min under HCOOH(200 ppm)/N_2 flow. The observed peaks were assigned to the carboxylic acid group (-COOH). The peak positions in the spectra and the profiles for formic acid adsorbed onto H-Y (Figure 8b) were in good agreement with those for toluene adsorbed onto H-Y treated with O_3 (Figure 7c–f). Therefore, the peaks in Figure 7c–f can be assigned to formic acid. When a mixture of 400 ppm O_3 in O_2 was introduced for 10 min, the peak at 1725 cm^{-1} decreased by approximately half of its initial intensity, and the peak at 1630 cm^{-1} increased significantly in intensity. The decomposition rate of formic acid was much lower than that of toluene under the same conditions. Therefore, the benzene ring was relatively easily decomposed on the H-Y surface compared to carboxylic acid. With reference to the IR spectra of H_2O (Figure 8d), the peak at 1630 cm^{-1} with increased intensity was assigned to H_2O the final product of formic acid oxidation.
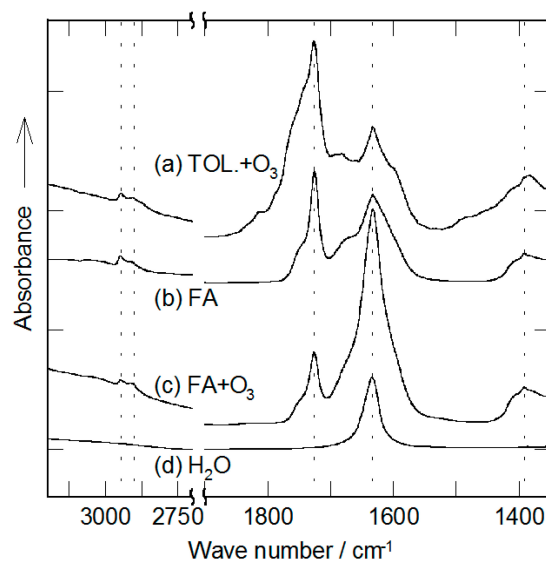

Figure 8. Infra-red spectra of (**a**) toluene adsorbed onto H-Y(1) after introducing O_3, (**b**) formic acid adsorbed onto H-Y, (**c**) after adducting O_3, and (**d**) H_2O adsorbed onto H-Y.

3. Experimental Section

3.1. Decomposition of Toluene (C7H8)

The configuration of the surface discharge reactor is shown in Figure 9a. A quartz tube (i.d.: 10 mm, thickness: 1.5 mm) was used as the dielectric barrier. A spiral platinum wire coil (70 turns/100 mm) with a 0.3 mm diameter was placed in contact with the inner wall of the barrier tube. A piece of copper foil was wrapped around the outside of the barrier tube as the ground electrode; the outer electrode length was 100 mm.
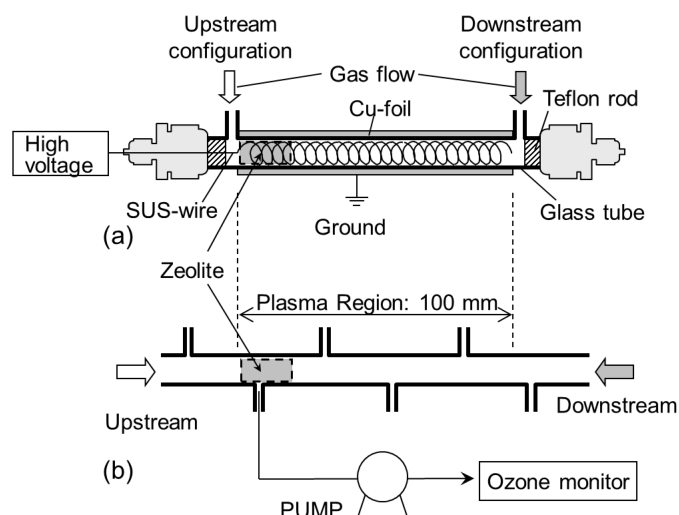
Figure 9. Configurations of (**a**) the zeolite hybrid reactor and (**b**) the reactor for monitoring the ozone distribution in the plasma region.

Zeolites (1 g) were packed into one end of the reactor. The reaction conditions were adjusted based on the flow direction and the position of the zeolites. The position of the zeolites was near the gas inlet in the upstream configuration and near the gas outlet in the downstream configuration.

The reactant gas consisted of 200 ppm toluene (C_7H_8), 0.5% H_2O, and 20.0% O_2, with N_2 making up the remaining fraction. It was fed at a flow rate of 500 cm^3/min into the reactor, where a high AC voltage was applied between the two electrodes. The plasma energy was supplied using an AC high-voltage neon transformer (24 kHz, NEON M-5; Lecip Co., Gifu, Japan) and the plug-in power was measured using a digital power meter (WT110; Yokogawa Electric Co., Tokyo, Japan). The input power was 5 W.

The plasma was cycled four times in 160 min (off for 30 min → on for 10 min → off for 30 min → *etc.*) (Figure 10), because cyclic operation improves energy efficiency by inducing periods of adsorption followed by plasma decomposition [8,13]. The concentrations of products such as COx were consistent during each plasma period. The experiment was carried out at room temperature. Under plasma operation, the reactor temperature was increased to approximately 60 °C.
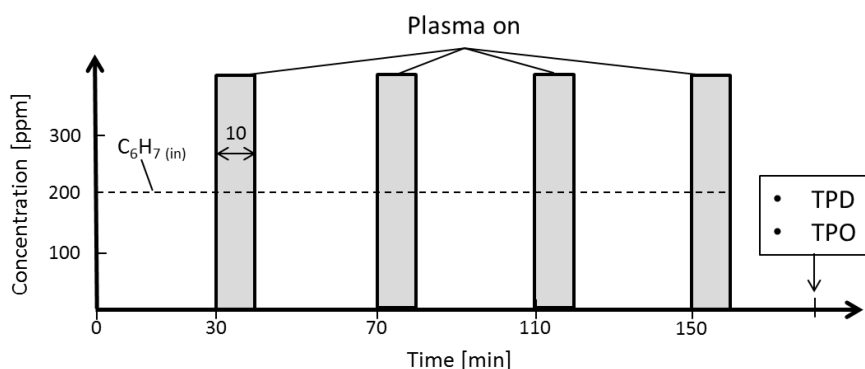

Figure 10. Plasma cyclic operation.

The effluent gas was monitored continuously using an FT-IR spectrometer (FTS135; Bio-Rad Laboratories, Hercules, CA, USA) equipped with a gas cell (2.4 m path, 125 cm^3 volume; Infrared Analysis Inc., Anaheim, CA, USA) and the total amounts of the products were calculated from their

integrated spectra. Under plasma operation, production of N_2O and HNO_3 was confirmed. The concentration of N_2O was approximately 60 ppm. An accurate concentration for HNO_3 could not be determined due to overlap of the FT-IR spectrum with that for H_2O. The amounts of adsorbed components on the zeolite were measured using temperature-programmed desorption and oxidation (TPD and TPO, respectively) after cyclical operation. For the TPD process, the zeolite was heated to 500 °C at a rate of 10 °C/min and held at that temperature under N_2 atmosphere. After the TPD process, the residual solid carbon was oxidized at 600 °C under synthetic air. Decomposition efficiency was calculated as follows:

$$C_7H_8 \text{ decomposition } (\%) = (C_7H_{8in} - C_7H_{8out} - C_7H_{8TPD})/(C_7H_{8in}) \times 100 \qquad (4)$$

where C_7H_{8in} and C_7H_{8out} are the total input and output of toluene, respectively. $(C_7H_8)_{TPD}$ is the amount of toluene desorbed from the TPD reactor, where the adsorbed toluene could be easily desorbed from the zeolite surface without noticeable decomposition. The carbon balance was estimated as follows:

$$\text{Carbon balance } (\%) = (CO_2 + CO + HCOOH)/7C_7H_{8decomposition} \times 100 \qquad (5)$$

Based on the relatively high carbon balance (Table 1), the influence of products other than those above, such as carbon deposition on the zeolite surface, was negligible. Thus, the product selectivity, where $X = CO$, CO_2, or $HCOOH$, was calculated as follows:

$$\text{Selectivity for } X \ (\%) = (X)/(CO_2 + CO + HCOOH) \times 100 \qquad (6)$$

Four types of zeolites were used in this study: A Na-forms of faujasite (Na-Y), two H-forms of faujasite (H-Y), an H-form of mordenite (MOR), and an H-forms of ferrierite (FER). These samples molded into pellets were purchased from Tosoh Co. (Tokyo, Japan) and Nikki-Universal Co. Ltd. (Tokyo, Japan). Quite similar V-I patterns were observed for all zeolites.

3.2. Measurement of the Ozone Concentration in the Reactor

A reactor with six branch pipes (Figure 9b) was used to measure the O_3 distribution in the plasma region at room temperature. The gas was sampled from each branch pipe using a diaphragm pump and O_3 was measured using an ozone-monitor (PG-620H; Ebara Jitsugyo Co., Ltd., Tokyo, Japan). The zeolite pellets (1.0–3.0 g) were filled in the area indicated by the dotted line. Dry air (20% O_2 and 80% N_2) was introduced into the reactor at a flow rate of 500 cm^3/min, and an input power of 2.0 W was applied.

3.3. Infrared Measurement of the Chemical Species Adsorbed onto the Zeolites

The IR spectra for chemical species adsorbed onto H-Y and FER were recorded using an FT-IR spectrometer (Spectrum 100; Perkin-Elmer Co. Ltd., Waltham, MA, USA) equipped with an IR cell for solid samples (Figure 11). The pellets were ground to a fine powder with an agate mortar and pestle, and the sample (0.043–0.044 g) was pressed into a thin disc 20 mm in diameter. The disc was inserted in the sample holder (Figure 11a) and the spectrum was measured using the transmission method. The sample could be moved to a heated position under desired gas flow conditions and to the measuring position at room temperature. The spectrum was measured at a resolution of 4.0 cm^{-1} and scan numbers of 200 using mercury cadmium telluride detector.
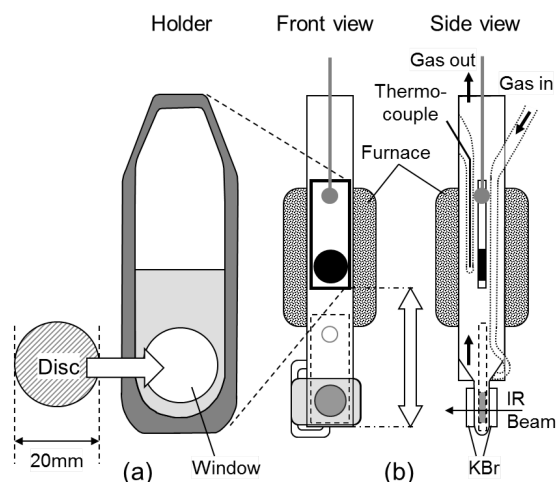
Figure 11. Configurations of (**a**) the sample holder and (**b**) the IR cell equipped with a furnace.

4. Conclusions

The reaction mechanism of the zeolite-plasma hybrid system for toluene decomposition was studied using gas and surface FT-IR analyses. The contributions of short-lived radicals and fast electrons to decomposition of adsorbed toluene were low. On the other hand, O_3 directly decomposed toluene adsorbed in the inner areas of the zeolite micropore because it has a long life time. O_3 provided the main mechanism of toluene decomposition in the zeolite-plasma hybrid system, unlike in metal-loaded zeolite-plasma systems. CO_2 selectivity was not improved by use of the bare zeolite, because H-Y zeolite does not retain active oxygen species on its surface through surface reactions of O_3. Gas-phase O_3 reacted with adsorbed toluene to form a ring cleavage intermediate that was slowly converted to formic acid. The decomposition rate of formic acid was much slower than that of toluene on the H-Y surface.

Author Contributions

Y.T., H.H.K., N.N. and A.O. designed the research; A.O. performed research; Y.T., H.H.K. and A.O. analysed data; Y.T. wrote, and all authors commented on the manuscript.

Conflicts of Interest

The authors declare no conflict of interest.

References

1. Oda, T. Non-thermal plasma processing for environmental protection: Decomposition of dilute VOCs in air. *J. Electrostat.* **2003**, *57*, 293–311.
2. Nunez, C.M.; Ramsey, G.H.; Ponder, W.H.; Abbott, J.H.; Hamel, L.E.; Kariher, P.H. Corona destruction—An innovative control technology for VOCs and air toxics. *J. Air Waste Manag.* **1993**, *43*, 242–247.
3. Yamamoto, T.; Futamura, S. Nonthermal plasma processing for controlling volatile organic compounds. *Combust. Sci. Technol.* **1998**, *133*, 117–133.

4. Sobacchi, M.G.; Saveliev, A.V.; Fridman, A.A.; Gutsol, A.F.; Kennedy, L.A. Experimental assessment of pulsed corona discharge for treatment of VOC emissions. *Plasma Chem. Plasma Process.* **2003**, *23*, 347–370.

5. Ogata, A.; Ito, D.; Mizuno, K.; Kushiyama, S.; Gal, A.; Yamamoto, T. Effect of coexisting components on aromatic decomposition in a packed-bed plasma reactor. *Appl. Catal. A* **2002**, *236*, 9–15.

6. Park, D.W.; Yoon, S.H.; Kim, G.J.; Sekiguchi, H. The effect of catalyst on the decomposition of dilute benzene using dielectric barrier discharge. *J. Ind. Eng. Chem.* **2002**, *8*, 393–398.

7. Oda, T.; Yamashita, R.; Haga, I.; Takahashi, T.; Masuda, S. Decomposition of gaseous organic contaminants by surface discharge induced plasma chemical processing spcp. *IEEE Trans. Ind. Appl.* **1996**, *32*, 118–124.

8. Oh, S.M.; Kim, H.H.; Ogata, A.; Einaga, H.; Futamura, S.; Park, D.W. Effect of zeolite in surface discharge plasma on the decomposition of toluene. *Catal. Lett.* **2005**, *99*, 101–104.

9. Kim, H.H.; Oh, S.M.; Ogata, A.; Futamura, S. Decomposition of benzene using Ag/TiO$_2$ packed plasma-driven catalyst reactor: Influence of electrode configuration and Ag-loading amount. *Catal. Lett.* **2004**, *96*, 189–194.

10. Futamura, S.; Einaga, H.; Kabashima, H.; Lee, Y.H. Synergistic effect of silent discharge plasma and catalysts on benzene decomposition. *Catal. Today* **2004**, *89*, 89–95.

11. Ogata, A.; Einaga, H.; Kabashima, H.; Futamura, S.; Kushiyama, S.; Kim, H.H. Effective combination of nonthermal plasma and catalysts for decomposition of benzene in air. *Appl. Catal. B* **2003**, *46*, 87–95.

12. Magureanu, M.; Mandache, N.B.; Parvulescu, V.I.; Subrahmanyam, C.; Renken, A.; Kiwi-Minsker, L. Improved performance of non-thermal plasma reactor during decomposition of trichloroethylene: Optimization of the reactor geometry and introduction of catalytic electrode. *Appl. Catal. B* **2007**, *74*, 270–277.

13. Han, S.B.; Oda, T.; Ono, R. Improvement of the energy efficiency in the decomposition of dilute trichloroethylene by the barrier discharge plasma process. *IEEE Trans. Ind. Appl.* **2005**, *41*, 1343–1349.

14. Hakoda, T.; Matsumoto, K.; Mizuno, A.; Kojima, T.; Hirota, K. Catalytic oxidation of xylene in air using TiO$_2$ under electron beam irradiation. *Plasma Chem. Plasma Process.* **2008**, *28*, 25–37.

15. Rousseau, A.; Meshchanov, A.V.; Roepcke, J. Evidence of plasma-catalyst synergy in a low-pressure discharge. *Appl. Phys. Lett.* **2006**, *88*, doi:10.1063/1.2164915.

16. Kim, H.H.; Kim, J.H.; Ogata, A. Microscopic observation of discharge plasma on the surface of zeolites supported metal nanoparticles. *J. Phys. D* **2009**, *42*, 135210.

17. Ogata, A.; Ito, D.; Mizuno, K.; Kushiyama, S.; Yamamoto, T. Removal of dilute benzene using a zeolite-hybrid plasma reactor. *IEEE Trans. Ind. Appl.* **2001**, *37*, 959–964.

18. Oh, S.M.; Kim, H.H.; Einaga, H.; Ogata, A.; Futamura, S.; Park, D.W. Zeolite-combined plasma reactor for decomposition of toluene. *Thin Solid Films* **2006**, *506*, 418–422.

19. Sano, T.; Negishi, N.; Sakai, E.; Matsuzawa, S. Contributions of photocatalytic/catalytic activities of TiO$_2$ and g-Al$_2$O$_3$ in nonthermal plasma on oxidation of acetaldehyde and co. *J. Mol. Catal. A Chem.* **2006**, *245*, 235–241.

20. Bulanin, K.M.; Lavalley, J.C.; Lamotte, J.; Mariey, L.; Tsyganenko, N.M.; Tsyganenko, A.A. Infrared study of ozone adsorption on CeO$_2$. *J. Phys. Chem. B* **1998**, *102*, 6809–6816.

21. Einaga, H.; Futamura, S. Catalytic oxidation of benzene with ozone over mn ion-exchanged zeolites. *Catal. Commun.* **2007**, *8*, 557–560.

22. Teramoto, Y.; Kim, H.H.; Ogata, A.; Negishi, N. Study of plasma-induced surface active oxygen on zeolite-supported silver nanoparticles. *Catal. Lett.* **2013**, *143*, 1374–1378.

23. Kim, H.H.; Sugasawa, M.; Hirata, H.; Teramoto, Y.; Kosuge, K.; Negishi, N.; Ogata, A. Ozone-assisted catalysis of toluene with layered ZSM-5 and Ag/ZSM-5 zeolites. *Plasma Chem. Plasma Process.* **2013**, *33*, 1083–1098.

24. Einaga, H.; Ogata, A. Benzene oxidation with ozone over supported manganese oxide catalysts: Effect of catalyst support and reaction conditions. *J. Hazard Mater.* **2009**, *164*, 1236–1241.

25. Kwong, C.W.; Chao, C.Y.H.; Hui, K.S.; Wan, M.P. Catalytic ozonation of toluene using zeolite and MCM-41 materials. *Environ. Sci. Technol.* **2008**, *42*, 8504–8509.

26. Chao, C.Y.H.; Kwong, C.W.; Hui, K.S. Potential use of a combined ozone and zeolite system for gaseous toluene elimination. *J. Hazard Mater.* **2007**, *143*, 118–127.

27. Sullivan, R.C.; Thornberry, T.; Abbatt, J.P.D. Ozone decomposition kinetics on alumina: Effects of ozone partial pressure, relative humidity and repeated oxidation cycles. *Atmos. Chem. Phys.* **2004**, *4*, 1301–1310.

28. Li, W.; Gibbs, G.V.; Oyama, S.T. Mechanism of ozone decomposition on a manganese oxide catalyst. I. In situ raman spectroscopy and ab initio molecular orbital calculations. *J. Am. Chem. Soc.* **1998**, *120*, 9041–9046.

29. Li, W.; Oyama, S.T. Mechanism of ozone decomposition on a manganese oxide catalyst. 2. Steady-state and transient kinetic studies. *J. Am. Chem. Soc.* **1998**, *120*, 9047–9052.

30. Ogata, A.; Shintani, N.; Mizuno, K.; Kushiyama, S.; Yamamoto, T. Decomposition of benzene using a nonthermal plasma reactor packed with ferroelectric pellets. *IEEE Trans. Ind. Appl.* **1999**, *35*, 753–759.

31. Kuroki, T.; Fujioka, T.; Okubo, M.; Yamamoto, T. Toluene concentration using honeycomb nonthermal plasma desorption. *Thin Solid Films* **2007**, *515*, 4272–4277.